ENVIRONMENTAL RESEARCH
LETTERS

PURPOSE-LED PUBLISHING™ Part of the ENVIRONMENTAL RESEARCH SERIES

LETTER • OPEN ACCESS

Energy production and inter-farm wake losses in future North Sea wind farms

To cite this article: R Borgers *et al* 2025 *Environ. Res. Lett.* **20** 074036

IOP Publishing Environ. Res. Lett. 20 (2025) 074036 https://doi.org/10.1088/1748-9326/add8a2

ENVIRONMENTAL RESEARCH
LETTERS

OPEN ACCESS

RECEIVED
29 October 2024

REVISED
25 March 2025

ACCEPTED FOR PUBLICATION
14 May 2025

PUBLISHED
13 June 2025

LETTER

Energy production and inter-farm wake losses in future North Sea wind farms

R Borgers[1,*], **J Meyers**[2] **and N P M van Lipzig**[1]

[1] Department of Earth and Environmental Sciences, KU Leuven, Leuven, Belgium
[2] Department of Mechanical Engineering, KU Leuven, Leuven, Belgium
[*] Author to whom any correspondence should be addressed.

E-mail: ruben.borgers@kuleuven.be

Keywords: offshore wind farms, mesoscale modeling, wake losses, Ostend Declaration, COSMO-CLM

Supplementary material for this article is available online

Abstract

The deployment of new wind farms in the North Sea is an essential part of Europe's transition to low-emission energy sources. Here, we use the mesoscale climate model COSMO-CLM to simulate the energy production of a realistic 92 GW wind farm expansion scenario and compare it with that of the wind farm distribution in 2024. The simulations indicate that added inter-farm wakes would cause the annual energy production of 25 out of 69 operational wind farms to decline by over 5%, with 13 of them experiencing reductions exceeding 10%. These annual losses are composed of intermittent wake periods characterized by large production deficits. For instance, the planned Princess Elisabeth zone in Belgian waters is expected to reduce the output of the existing Belgian wind farm cluster by more than 15% during one out of every five 24 h periods with high production potential ($\bar{V} > 9\,\mathrm{ms}^{-1}$). Despite these enhanced inter-farm interactions, we find that the overall capacity factor over the basin increases by 1.6%pt after expansion due to the deployment of next-generation turbines and installation at low capacity densities in high-resource zones. However, negative impacts are highly region-dependent and many wind farms may face substantial losses. Although more validation studies are recommended to further constrain the uncertainty on the presented results, this work demonstrates the need for a coordinated wind farm expansion strategy, especially because spatial constraints are expected to intensify on the path to surpassing 200 GW of capacity in the North Sea by 2050.

1. Introduction

With global greenhouse gas emissions reaching an all-time high in 2023, an urgent transition to low-emission energy systems is essential to limit adverse effects [1]. The offshore wind energy sector is a key player in this transition, having achieved a global capacity of over 72 GW in 2023—more than ten times the capacity in 2013 [2]. In Europe, plans are underway for another tenfold increase in offshore capacity to achieve climate neutrality by 2050 [3]. However, the urgency of the situation has also led to ambitious short-term growth targets, such as the more than threefold increase in the capacity over the North Sea basin by 2030, as outlined in the Ostend Declaration of 2023 [4].

The wind conditions at a wind farm site are determined by the large-scale atmospheric flow and the interaction with local and regional surface characteristics. The wind field can vary over a broad range of timescales, causing both intra-day and inter-annual variations in energy production [5, 6]. Furthermore, the efficiency of wind farms is influenced by the inter-turbine spacing, as upstream turbines create wakes of reduced momentum which recover gradually with distance [7]. In the same way, adjacent wind farms have been observed to impact each other through farm-scale wakes [8]. These farm wakes have

been observed to extend more than 50 km downstream from a wind farm [9, 10], and are gaining importance as offshore zones become more densely built. Research into these wakes has employed various modeling tools, including analytical wake models [11], Large Eddy Simulations (LES) [12] and mesoscale atmospheric models [13]. Mesoscale models are able to simulate regional-scale wind farm effects over climatologically representative periods while accounting for the full (thermo)dynamic variability of the planetary boundary layer (PBL). As a result, these models have been used to quantify long-term losses due to inter-farm wakes [14, 15], the associated impact on the power grid balance [16] and how these losses could be mitigated by employing different rotor heights in neighboring wind farms [17]. Furthermore, mesoscale simulations have been applied to study the long-term efficiency of projected wind farm scenarios and the losses associated with large-scale wake effects [18–22]. However, these studies have mostly been done for long-term wind farm scenario projections that include a large degree of uncertainty. Several studies have shown that intra-farm wake losses are generally greater than inter-farm wakes losses on the long term [23, 24]. However, since inter-farm wake interactions are constrained to specific wind directions, they are intermittent and can have a very large impact on operational timescales.

In this study, we quantify the energy production and efficiency of a projected, near-future (2030) North Sea wind farm distribution which includes many wind farms that are in the (pre-)construction phase or are expected to be built by the end of 2030. We analyze these findings per exclusive economic zone (EEZ) and discuss the role of spatial constraints, next-generation turbines and the background wind climate. Furthermore, we provide a detailed quantitative analysis of inter-farm wake losses for a set of selected wind farms and analyze them for specific wind directions, wind speeds and timescales (6 h to one week). To achieve this, we rely on three 10-year climate simulations performed using the mesoscale model COSMO-CLM, allowing us to include inter-annual variability in our analyses. Additionally, we provide in the appendix a comparison of aggregated energy production data for the Belgian offshore wind farms with the simulation output to better constrain the uncertainty on energy production estimates derived from our mesoscale modeling approach. The design of the wind farm expansion scenarios and the COSMO-CLM setup are discussed in the following section.

2. Data and methods

2.1. COSMO-CLM model setup

The climate model that was used for the atmospheric simulations is COSMO-CLM version 5.0-15, which is a non-hydrostatic and fully-compressible model suitable for mesoscale simulations at the meso-γ scale. This model has been used extensively for modeling of wind resources [5, 25–29] and wind farm-atmosphere interactions [18, 19, 30, 31]. The model configuration and domain setup correspond to the one described in Borgers *et al* [19]. The model domain has a horizontal grid increment of ∼2.8 km, with boundaries situated more than 150 km away from most wind farms to ensure sufficient spatial spin-up (figure 1). In the vertical, 61 levels were used, with level spacing gradually increasing from 20 m at the surface up to the model top of 22 km. The model setup used here was validated in the study of Borgers *et al* [19] in terms of the capability to model the wind statistics between 10 m and 300 m above mean sea level (MSL). Their comparison to multi-year measurement series from wind masts, wind lidars and satellite measurements showed a very good agreement in the long-term wind speed and wind direction statistics in addition to the intra- and inter-annual variations.

To simulate the wind farms and their interaction with the atmosphere, the model was extended with the Fitch wind farm parametrization (WFP) [32]. In this parametrization, the thrust of wind turbines in a model grid cell is approximated by a bulk reduction in mean flow kinetic energy which is distributed over the vertical layers that coincide with the turbine rotor. Furthermore, the fraction of this kinetic energy that is not converted into electrical energy is reintroduced into the atmosphere as a bulk source of turbulence (TKE), because electro-mechanical losses are neglected. To realistically represent the wind farms in this study, the latest COSMO-CLM implementation of the Fitch WFP was updated so that the turbine dimensions, density of turbines and the performance curves (C_p and C_t) could vary spatially. Mesoscale models using the Fitch WFP have been found to skillfully simulate *in situ* and airborne wind speed measurements in the wake of a wind farm and inside wind farms [18, 33–36]. Other studies have found a good agreement with higher-resolution RANS and LES simulations [31, 37]. However, it is important to note that there exist very little validation of energy production derived from mesoscale WFPs. Performance could be impacted by the fact that some mechanisms are not represented in the model, e.g. subgrid-scale turbine wake interactions, downtime and curtailment of turbines and the dependence of turbine performance on turbulence intensity.

The simulations in this work were done for a 10-year period. Based on an analysis of 100 m winds from ERA5 over the North Sea, it was found that a subperiod of 10 years can closely match the wind statistics for the period 1991–2020. This was determined according to the procedure outlined in Borgers *et al* [19]. The boundary conditions for the simulations were derived from the ERA5 reanalysis for the most

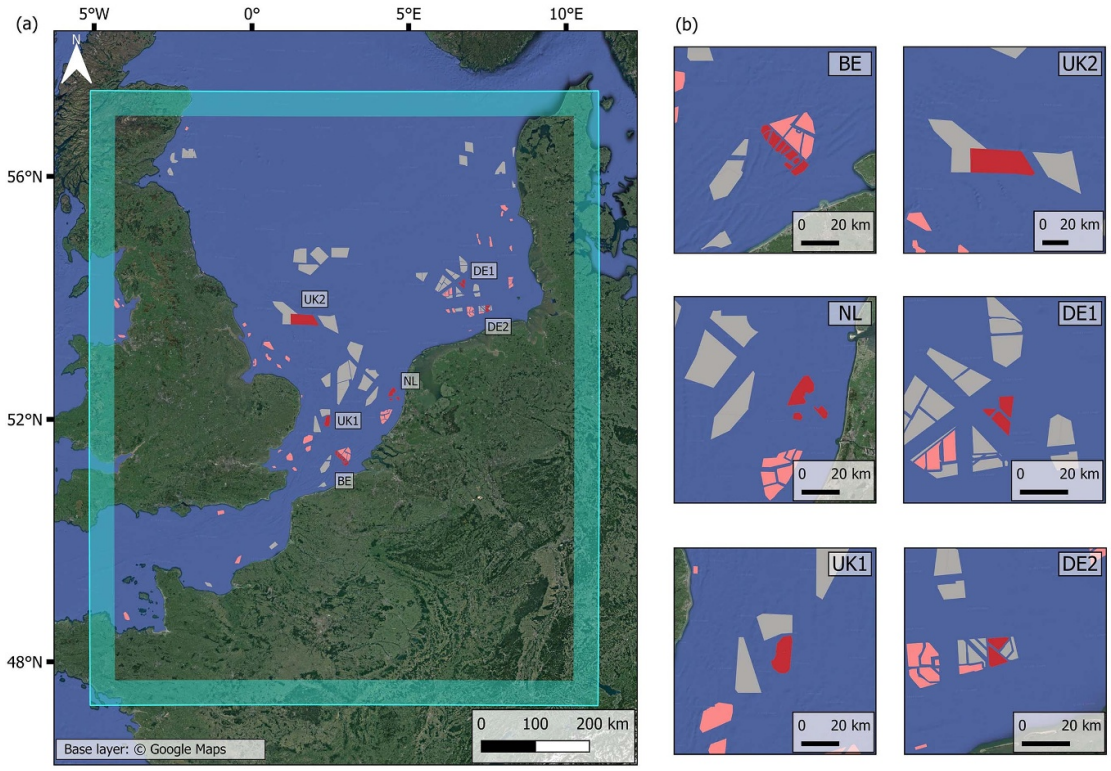

Figure 1. Geographic overview of the study area. (a) Map showing the edges and relaxation boundary zone of the simulation domain (cyan), the operational scenario of Q2 2024 (pink and red) and additional wind farms planned to be operational by 2030 (grey). The six wind farm groups in red are analyzed in more detail with respect to additional inter-farm wakes caused by the commissioning of the new wind farms (more information in table A1). (b) Zoomed maps of the region around the six wind farm groups.

representative sub-period, which was found to be 2000–2009 (see supplementary figure S1). The simulations were started one year earlier to allow spin-up of the included soil model, TERRA-ML. Three simulations were performed: a reference simulation without wind farms and two wind farm simulations. The corresponding wind farm scenarios will be described in more detail in the next subsection.

2.2. Wind farm scenarios

Two wind farm scenarios were developed for this study: one representing the operational situation in Q2 2024, and a projected scenario for the year 2030. The corresponding COSMO-CLM simulations will be referred to as WF24 and WF30, respectively. The reference simulation without wind farms will be abbreviated to NOWF. The georeferenced vector files used for the construction of the WF24 scenario were mostly obtained from the European Marine Observation and Data Network (EMODnet) [38]. Some additional zones for Belgium were collected from the Royal Belgian Institute for Natural Sciences (RBINS) [39]. For the wind farms located in the Irish Sea, the zone extent was clipped to avoid having wind farms in the lateral relaxation zone of the model (figure 1). The total capacity of the final WF24 scenario was approximately 25.5 GW.

The WF30 projection consists of this WF24 scenario expanded with a set of new wind farms in each country's EEZ. The addition of new wind farms for each EEZ was motivated by the pledges formulated in the Ostend Declaration [4]. The pledged additional capacity for 2030 raised the total capacity from 25.5 to 92 GW, which corresponds to ∼30% of the aspired capacity addition by 2050. To construct the scenario, the planned growth per country was matched with specific wind farm development projects based on the scheduled commissioning dates for these projects. With some exceptions, all added wind farm zones were taken from the EMODnet dataset [38]. For Germany and Denmark, insufficient zones could be identified for which the commissioning date was announced to be before 2031. Therefore, other planned zones were added to match the planned growth for 2030. For Denmark, additional zones were constructed for the Nordsøen tender zones from the turbine data used in the study of Hahmann *et al* [40]. For Germany, a few additional planned zones were obtained from the study of Slavik *et al* [41]. No windfarms from the WF24 scenario were decommissioned in the WF30 scenario, because all of them could still

be operational in 2030 given that they were all built after 2005 and the lifetime of windfarms can reach 25 years [42]. Furthermore, these older windfarms might get a life extension or might be repowered instead of being removed [43].

The Fitch WFP relies on five inputs to describe the wind farm properties in a grid cell: rotor radius, rotor hub height, C_t curve, C_p curve and the turbine density. For the wind farms of the WF24 scenario, the rotor radius and hub height were easily retrieved online. Turbine density was inferred from the turbine count and the wind farm surface area specified in the EMODnet dataset. More than half of the wind farms included in the WF24 scenario were also included in the study of van Stratum *et al* (2022) and they have made the C_p and C_t curves linked to these wind farms available [44]. For that specific set of farms, the 16 different C_p-C_t couples were taken over from their work. However, for the other WF24 wind farms, the C_t and C_p curves could not be found. Therefore a heuristic approach was used to select the best match from a set of available C_p and C_t curves for each wind farm. This approach was developed based on the empirical observation that the ratio of the turbine rating to the rotor diameter is strongly linked to the shape of the C_p curve. The approach relies on the wind turbine power equation:

$$P = \frac{1}{2}\rho A C_p(V)\, V^3 \tag{1}$$

where P is the power output, ρ is a standard air density of 1.225 kg m^{-3}, A is the turbine rotor area, V is the wind speed and C_p is the power coefficient that is a function of wind speed. For each available C_p curve, a rated power was derived by combining it with the known turbine rotor area in (1). This list of rated powers was then compared with the known turbine rating at the wind farm, from which a best match was selected (together with the corresponding C_t curve). In this study, the 16 different C_p–C_t couples of van Stratum *et al* [44] were used in combination with the C_p–C_t couples of three reference wind turbines, namely the NREL 5 MW, DTU 10 MW and IEA 15 MW turbines [45–47]. In many cases, the best match gave a rated power that was within 5% of the known turbine rating, whereas the worst match would differ by more than 50% (e.g. supplementary figures S2 and S3). Any remaining under- of overestimation of the turbine rating due to the approximation approach was corrected for by a slight increase or decrease of the turbine density so that the correct farm capacity and capacity density was retained.

For the additional wind farms in WF30, the turbine specifications were sometimes already announced, in which case the rotor radius and hub height were set to match this turbine. In most cases, also the turbine density could be derived from the announced farm capacity and turbine rating. For these wind farms, C_p-C_t curves were determined with the previously described approximation approach. In the case where no turbine specifications could be retrieved, the wind farm was equipped with the specifications of the IEA 15 MW reference wind turbine, because projects after 2025 are planning to use turbines of 15 MW rating [48, 49]. For the few zones where only the area was available, the density of the IEA 15 MW turbines was set to match a high-end, planned capacity density for that EEZ: for the additional zones of Germany and Denmark, capacity densities of 12 and 6 MW per km^{-2} were chosen, respectively [38, 50, 51]. The wind farm scenarios can be downloaded via the KU Leuven Research Data Repository [52].

The additional inter-farm wake losses in WF30 compared to WF24 were studied in-depth for six wind farm groups (figure 1). These six groups were chosen based on their differences in terms of the background wind climate, capacity density, turbine specifications and distance from the new WF30 wind farms. A detailed overview of these groups and the new neighbors in WF30 is available in table A1 of the appendix.

3. Results

3.1. Overall changes in energy production

The domain-integrated capacity factor for WF30 is on average slightly larger than for WF24, notwithstanding the intensification of inter-farm wake losses in WF30 (figure 2(a)). For the wind farms common to both scenarios, the energy production is reduced by ∼4% in the WF30 scenario compared to WF24 (figure 2(b)). Although a large share of the WF24 wind farms does not experience significant losses in the WF30 scenario, 25 out of the 69 operational wind farms have an average AEP loss of more than 5% and for 13 of these the loss exceeds 10% (see supplementary table S1 and S2). As the overall efficiency of WF30 is larger than WF24, other effects more than compensate the inter-farm wake losses experienced by both old and new wind farms in WF30. First, 41 out of the 57 added wind farms were equipped with the 15 MW RWT, which is associated with higher capacity factors due to the increase of wind speed with height and the low rated wind speed [19]. Second, much of the added capacity is added farther from the coast, where the background wind resource is also higher (see supplementary figure S4). And third, a large part of the added capacity (mostly for the United Kingdom) is constructed at low capacity densities (<4.5 MW per km^{-2}) which is associated with lower internal wake losses.

The mean annual capacity factor for the WF30 simulation varies substantially across the different EEZs (table 1). This is the combined effect of the background wind climate and the properties of the turbines, the wind farms and the inter-farm configurations. For example, the Danish wind farm zones are characterized by a higher background wind resource,

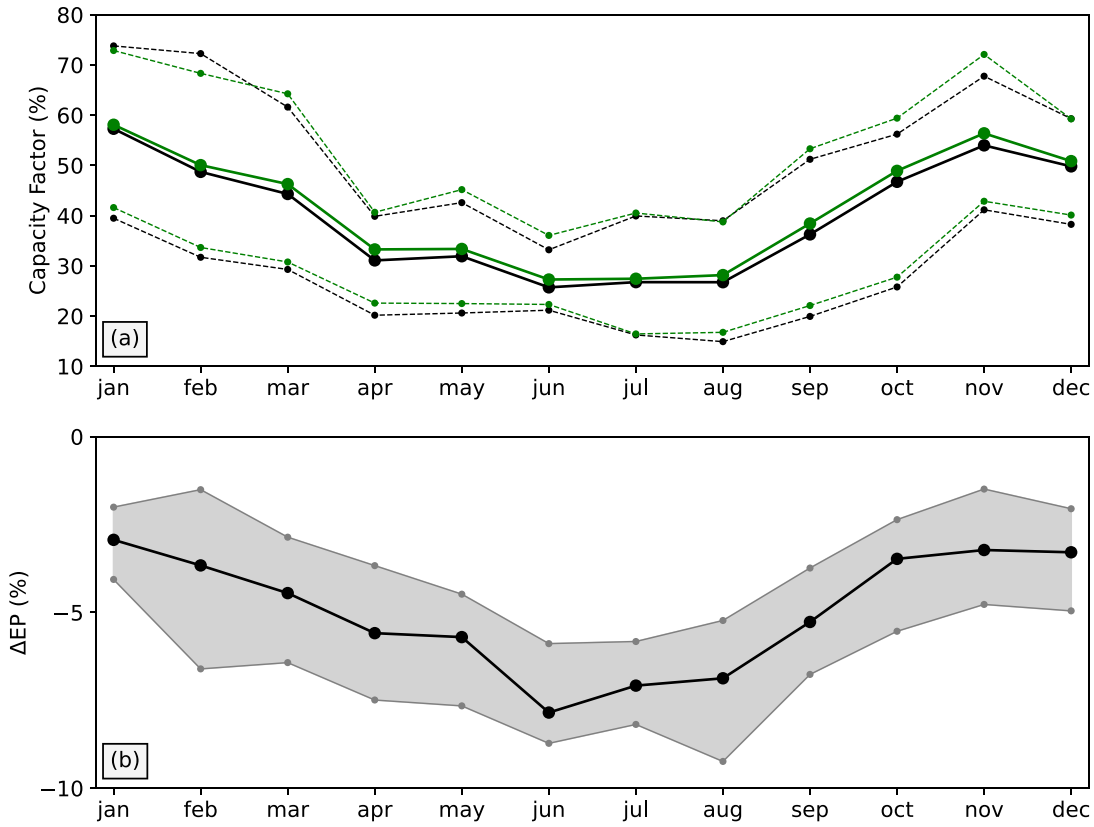

Figure 2. (a) Annual cycle of the monthly capacity factor of the complete wind farm fleet. Black: WF24, Green: WF30. Full lines represent the average monthly capacity factors over the simulation period 2000–2009. Dashed lines represent the minimum and maximum monthly capacity factor for 2000–2009. (b) Relative difference in the energy production of the wind farms common to both simulations (WF30 minus WF24). Black line: mean difference per month over 2000–2009. Grey lines: minimum and maximum difference per month over 2000–2009.

mostly larger turbines and lower capacity densities than the Belgian wind farm zones which translates to a substantial difference in capacity factor. The expansion of the wind farms of the United Kingdom is characterized by low capacity densities and ample space in high-resource regions, which translates to a higher capacity factor than in WF24. In contrast, the expansion of the German wind farms is characterized by high capacity densities and limited space, leading to a drop in capacity factor. Furthermore, the WF30 AEP is more stable over the years in zones with higher capacity factors. For example, the minimum AEP for Germany is 15.5% lower than the mean AEP, whereas this is only 10.8% for Denmark.

3.2. Impact on selected existing wind farms

Six operational wind farm groups (see figure 1 and table A1) are now analyzed in terms of the expected future decrease in energy production due to inter-farm wake losses (table 2). The AEP reduction for UK1 is similar to that for NL, despite the new wind farms around UK1 being closer and disturbing a larger sector. This is due to the higher capacity density of the new wind farms around the NL wind farm group than of the new wind farms around UK1 and also due to the fact that northerly winds do not occur often at the UK1 site so that the impact of the farm wakes coming from the new wind farm to the north is limited. Similarly, inter-farm configuration, capacity density, and wind statistics also explain the added inter-farm wake losses observed in the other wind farm groups. It is important to note that the losses are smaller on average than the losses already present in the WF24 simulation compared to NOWF, which originate mainly from within-farm or within-group wake effects. However, as the added inter-farm effect in WF30 is intermittent, it can become more important on shorter timescales. Moreover, as the inter-farm deficit is superposed on the intra-farm effect it can lead to large additional production losses due to the non-linear response of the turbines to wind speed changes. The inter-annual variability in the annual production deficits is limited, as the standard deviation over the 10 years is approximately an order of magnitude smaller than the average annual deficit (see also supplementary figure S6).

The inter-farm obstruction effect is clearly much larger than the previously discussed magnitudes which were not filtered for direction (figure 3). The operational BE group is strongly disadvantaged by the planned Princess Elisabeth offshore zone, more so because the obstruction occurs for the frequent

Table 1. Overview of the capacity, AEP and capacity factor values over the 10 years for the complete WF30 distribution and for each EEZ separately. The last column shows the absolute change in capacity factor from WF24 to WF30.

		AEP (TWh)			CF (%)			
EEZ	Capacity (GW)	mean	min	max	mean	min	max	$CF_{30} - CF_{24}$ (%pt.)
All	92	335.9	295.5	361.2	41.5	36.5	44.5	+1.6
France	2.5	9.4	8.6	10	42.1	38.6	45.1	+0.9
Belgium	5.8	17	14.7	18.8	33.8	29.2	37.1	+0.5
Netherlands	21	70	60.5	76.4	38.0	32.8	41.4	+1.9
United Kingdom	31	126.7	115.8	135.7	46.3	42.4	49.5	+4.4
Germany	26.4	90.2	76.2	98.6	39.5	33.4	43.1	−2.7
Denmark	5.2	24	21.4	25.4	52.4	46.8	55.3	+6.0

Table 2. Overview of the wind resource and energy production for the six wind farm groups. The NOWF mean wind speed at hub height represents the background wind resource averaged over the area of the wind farm group and over the complete simulation period. The difference in AEP is between the WF30 and WF24 simulation.

	$\overline{V_h}$ (ms^{-1})	Capacity factor (%)			$\overline{AEP}$ (TWh)		
Wind farm group	NOWF	NOWF	WF24	WF30	WF24	WF30	$\overline{\Delta AEP}$ (%)
BE	9.1	49.4	33.3	30.4	6.9	6.3	−8.5
NL	9.5	55.2	43.9	41.8	3.9	3.7	−4.6
UK1	9.5	53.3	43.6	41.2	2.7	2.6	−5.4
UK2	9.9	56.2	43.1	41.7	2.9	2.8	−3.3
DE1	9.8	55.1	42.6	35.2	2.6	2.1	−17.3
DE2	9.8	59.2	44.0	35.5	2.4	1.9	−19.3

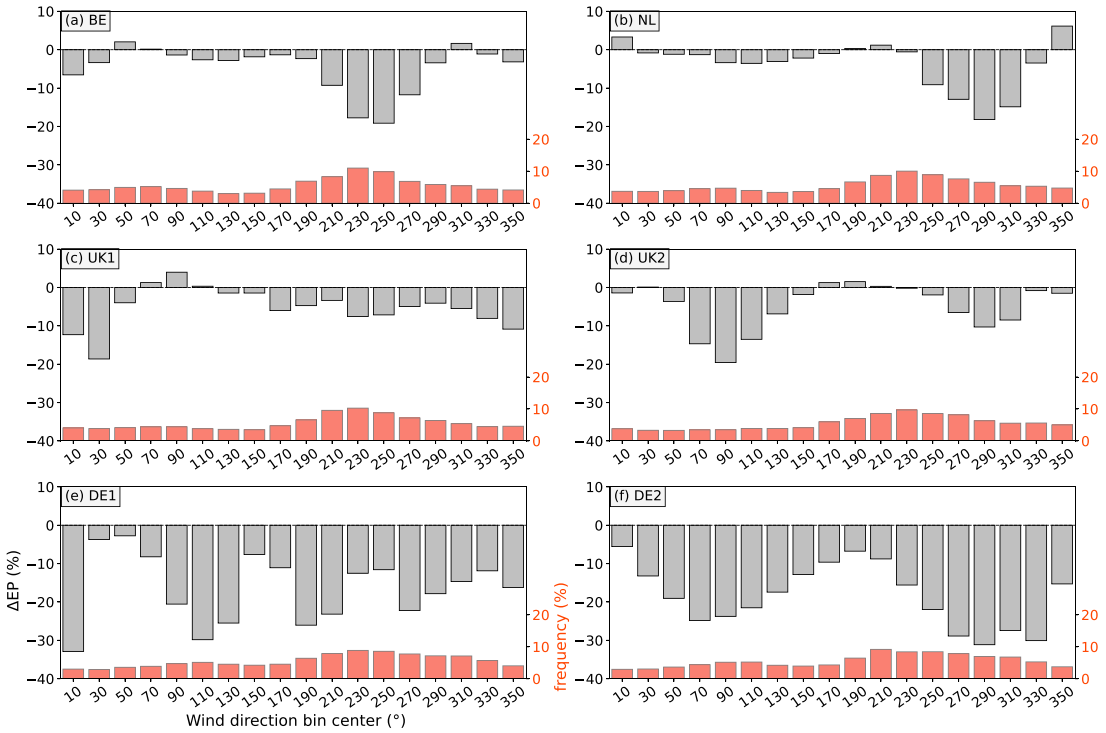

Figure 3. Grey bars: long-term difference in energy production per wind direction bin (20°) for six wind farm groups common to the WF24 and WF30 simulations. Light orange bars: Long-term frequencies of the different wind direction bins. The wind direction was derived from the background simulation, NOWF.

southwesterlies so that the impact on the AEP is large (see table 2). For other clusters, some of the obstruction occurs for infrequent wind directions (figure 3) that are also characterized by lower wind speeds (not shown), so that the impact on AEP is limited. For some wind farm groups and wind directions, long-term augmented production can even be recognized for WF30 compared to WF24. This seems to be the consequence of lateral flow speed-up around the new wind farms caused by their upwind flow blockage

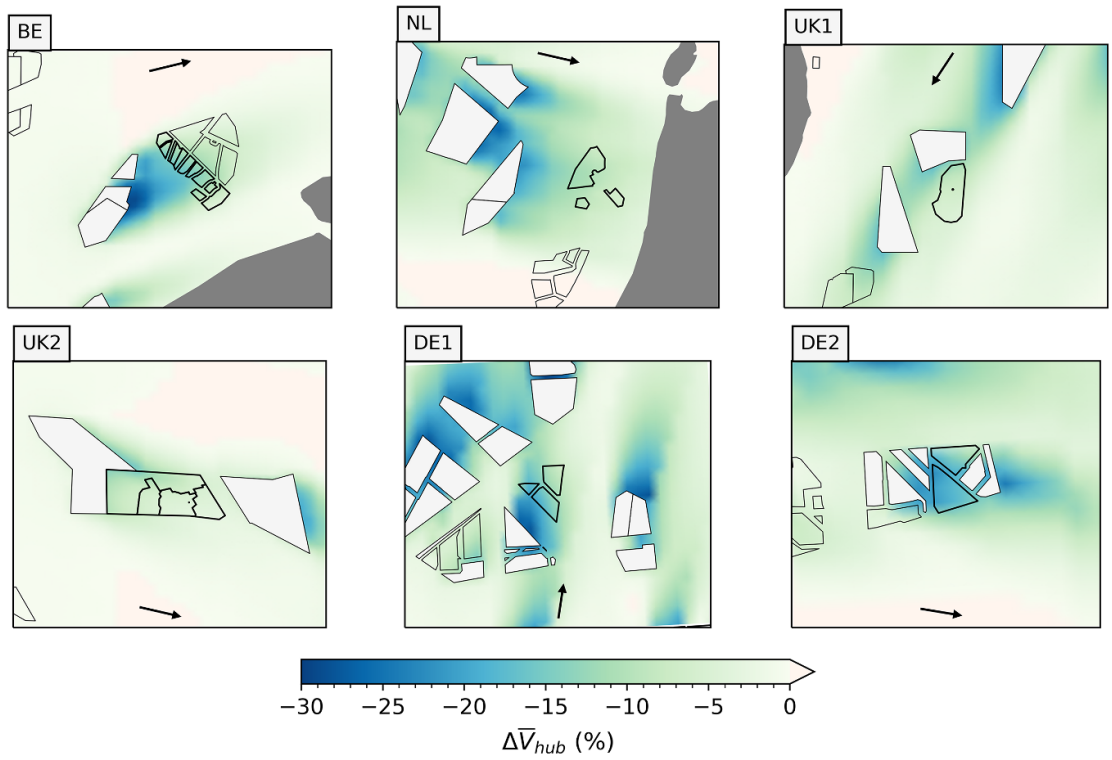

Figure 4. Time-averaged wind speed deficit at hub height (WF30 − WF24) for a disturbed wind direction range (20°) over the simulation period (2000–2009). The corresponding wind direction bin centers (black arrows) are 250° (BE), 290° (NL), 30° (UK1), 290° (UK2), 190° (DE1) and 290° (DE2). Winds in these sectors are disturbed by added wind farms and occur frequently, except for UK1. The WF24 wind farms are indicated with black contours, including those part of the six analyzed wind farm groups (bold) and others (thin). New wind farms in WF30 are indicated by white polygons. For the properties of the wind farm groups, consult table A1.

and positively impacts the energy production of the existing wind farms for these wind directions. This effect has been described in detail based on LES [12], but a more detailed inspection of our simulations is required to confirm this.

To illustrate the dependence of the inter-farm wake effect on the upwind capacity density and the inter-farm spacing, figure 4 shows the 10-year mean wind speed deficit at the inflow edge of the WF24 wind farms for a disturbed wind direction range. The UK1 and UK2 groups clearly benefit from the low upwind capacity densities, whereas the negative impact on the NL group is limited by the 20 km spacing from the wind farm to the west.

To assess the impact of inter-farm wake losses on shorter timescales, the energy production difference was analyzed through a sliding window over the simulation period, with a focus on high-resource periods ($\bar{V} > 9\,\mathrm{ms}^{-1}$) (figure 5). Energy production losses on shorter timescales can be several times larger than the long-term losses (see table 2). For the BE (DE1) wind farm group, more than 20% of the high-resource 24 h periods are subject to an energy loss larger than 15% (30%) compared to the WF24 simulation (figure 5). For BE, a small portion of periods have an augmented production in WF30, which is likely the consequence of the previously discussed lateral flow speed-up effect around the new wind farm zone under specific wind directions associated with the flow blockage in front of the new zone.

Note that the probability of higher losses is inversely related to the background wind speed, i.e. for lower wind speeds, wind speed changes are more likely to cause strong changes in power production due to the non-linear shape of the turbine power curves (see supplementary figure S9). The energy production of the BE (DE1) cluster is reduced by more than 20% for more than 1 in 5 (3 in 5) six-hour periods with background wind speeds between 9 ms^{-1} and 13 ms^{-1}. This also means that the energy production in zones characterized by higher wind speeds is inherently less sensitive to inter-farm obstruction.

4. Discussion

The changes in energy production shown here depend strongly on the quality of the simulated intra- and inter-farm wakes. Idealized COSMO-CLM simulations have shown that the impact of the wind farm forcing on vertical profiles of wind and TKE in a wind farm grid cell are captured reasonably well in comparison to LES [31]. Additionally, a reasonable agreement in wind deficits was found in terms of the farm wake deficit compared to aircraft measurements [18]. In supplementary figure S11 we have added a comparison of simulated vertical wind profiles with those

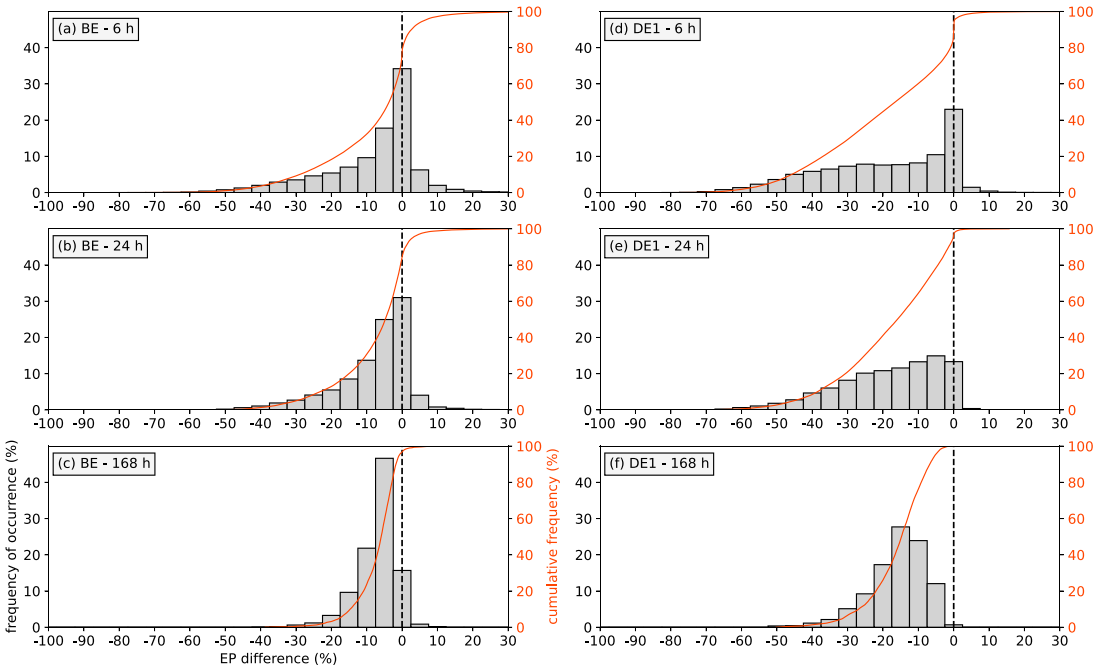

Figure 5. Grey bars: histogram of the difference in energy production at temporal window sizes of 6, 24 and 168 h, for two wind farm groups (BE and DE1) common to WF24 and WF30. Light orange line: cumulative distribution function of the histogram. The histogram is constructed based on a sliding window analysis over the simulation period 2000–2009. In the case that the window-averaged background wind speed was below 9 ms^{-1}, the data point was omitted (∼50%) in order to focus on periods with significant production potential.

measured by the Borssele wind lidar over 2016 near three Belgian wind farms. As the agreement varies strongly over the three wind farms, the analysis is not conclusive in terms of how well the farm wake deficit is modeled by COSMO-CLM.

It is encouraging that the simulated impacts of intra- and inter-farm wakes on AEP and CF of the operational Belgian cluster are similar to what has been simulated with WRF (incl. the Fitch WFP) [24], as several studies have found that WRF adequately captures wake deficits inside and downwind of wind farms [33, 36, 37, 53]. In contrast, analytical wake models have simulated smaller losses for this cluster [11], but this can be linked to the overly high farm wake recovery rates that have been identified for these models [37, 54]. Nonetheless, more in-depth validation studies are needed for COSMO-CLM which quantify the errors in intra- and inter-farm wake deficits and the dependence on horizontal and vertical resolution and model setup choices.

To our knowledge, no detailed comparative studies with energy generation data exists for mesoscale models, but Pryor *et al* (2020) have shown how wind farm capacity factors derived from WRF can differ by up to 10%pt for different setup choices in terms of the horizontal and vertical resolution and the WFP scheme [55]. Our comparison with four years of energy production data for the Belgian offshore wind farm cluster reveals an average underestimation of the annual CF of 2.6%pt by the model, which corresponds to ∼7.3% in the AEP (appendix B). Based on a deeper inspection, it is clear that compensating errors are present and that COSMO-CLM overestimates the intra-farm wake deficit, which is partially compensated by assuming 100% availability and no curtailment. Yet, the impact of model biases on production metrics are expected to be large for the Belgian wind farm cluster as this large cluster has a very high capacity density and a relatively high fraction of the background wind speeds are below or near the rated wind speed.

Finally, it is likely that the employed wind farm expansion scenario will not be exactly realized by the end of 2030, which is evidenced by some wind farm development projects being halted [56]. Also, for the wind farms for which we assumed the IEA 15 MW turbine and an EEZ-specific capacity density the actual properties will most likely deviate from our assumptions. But, because we mainly include wind farms for which development is underway with most specifications announced, and recent installations already using 13 MW turbines (e.g. [57]), we believe that our analyses remain highly relevant for the build-out of wind farms in the North Sea in the coming years.

5. Concluding remarks

Motivated by the ambitious near-term growth targets for the North Sea wind farm ensemble, we have performed a set of 10-year simulations with COSMO-CLM to quantify the energy production and efficiency of a realistic 92 GW wind farm projection.

For a large fraction of the wind farms operational in 2024, we found a substantial increase in inter-farm wake losses due to the expansion. For 13 out of 69 operational wind farms (mostly Belgian and German), these added inter-farm wake losses exceed 10% and even surpass 18% for a few wind farms in the German EEZ. Moreover, due to their intermittent nature, inter-farm interactions can cause short-term (6 h–24 h) losses that are more than three times the annually-integrated deficit, even under high-resource conditions (background wind above 9 ms^{-1}). However, losses associated with inter-farm wakes tend to be small at background wind speeds above 13 ms^{-1} and nearly negligible above 15 ms^{-1}.

The reduced efficiency of the 2024 wind farm subset leads to a 4% decrease in their energy production. However, this is more than compensated by other factors, as we found a 1.6%pt increase in the total capacity factor in comparison to the present-day scenario of 25.5 GW. This is primarily due to the deployment of next-generation 15 MW turbines and the construction of wind farms with low capacity densities in high-resource regions (mainly in the EEZ of the United Kingdom). However, efficiency changes vary across EEZs, with a smaller increase (Belgium) or even a decrease (Germany) where spatial constraints are largest.

Based on a comparison of the COSMO-CLM output with aggregated energy production data of the Belgian offshore wind farm cluster for 2021–2024, we find a consistent underestimation of the annual capacity factor of ∼2.6%pt, or 7.3% on the AEP. Yet, the impact of model biases on production metrics is likely on the higher end for the Belgian cluster, so these estimates cannot simply extrapolated to other wind farms. To further constrain the uncertainty on the presented results, in-depth validation studies of COSMO-CLM are required that assess the quality of simulated intra- and inter-farm wakes and energy production estimates.

Based on our findings, we recommend that stakeholders in wind farm development projects carefully consider the potential impacts of inter-farm wake interactions in wind farm planning, but also on operational timescales. Cooperation between wind farms, such as through farm wake steering, could be considered to reduce such losses [58]. More broadly, the expansion of wind farm zones should be carried out in a coordinated manner, where wind farm operators and neighboring states collaborate to find balanced solutions in areas where space is limited. This is particularly important given the regulatory gaps identified regarding cross-border farm wake effects [59], and because spatial constraints will become even more important on the way to the 2050 development targets.

Data availability statement

The COSMO-CLM simulation output used in this study can be downloaded through a GLOBUS interface. A detailed description on how to download the data is provided on the website of the FREEWIND project [60]. In addition to the simulations presented here, there are additional simulations available for 2050 wind farm scenarios. Furthermore, the wind farm scenarios used in this study are available for download via the KU Leuven Research Data Repository [52]. Finally, the updated wind farm parametrization code developed in the context of this study is also available through Zenodo [61].

Acknowledgments

This research has been supported by the Project FREEWIND, funded by the Energy Transition Fund of the Belgian Federal Public Service for Economy, SMEs, and Energy (FOD Economie, K.M.O., Middenstand en Energie). The computational resources and services in this work were provided by the VSC (Flemish Supercomputer Center), funded by the Research Foundation Flanders (FWO) and the Flemish government department EWI.

Appendix A. Overview table of the six wind farm groups

Table A1. Description of the six operational wind farm groups for which the impact of additional inter-farm wakes is studied. The abbreviation CD stands for capacity density. The overbar denotes that it is the area-weighted mean capacity density.

	Wind farms in group			New neighbors in WF30	
Group name	names	$\overline{\text{CD}}$ (MW km^{-2})	total capacity (MW)	names	$\overline{\text{CD}}$ (MW km^{-2})
BE	C-Power, Belwind, Nobelwind, Northwind, Seamade, Rentel, Norther, Northwester 2	12.7	2261	Princess Elisabeth Zone (PEZ)	12.5
NL	Hollandse Kust Noord, OWF Prinses Amalia, OWF Egmond aan Zee	5.8	990	Hollandse Kust West, IJmuiden Ver	8
UK1	East Anglia One	4.4	710	East Anglia One North, East Anglia Two, East Anglia Three	3.5
UK2	Hornsea Project 1,2	3.3	2620	Hornsea Project 3,4	2.3
DE1	GlobalTech I, EnBW Hohe See, EnBW Albatros	11	1010	EnBW He Dreiht, Nordlicht, Bard Offshore I, N-10.1, N11.1, N9.2, ...	12
DE2	Gode Wind 1 and 2	8.8	610	Nordsee One, Nordsee, Gode Wind 3	12.8

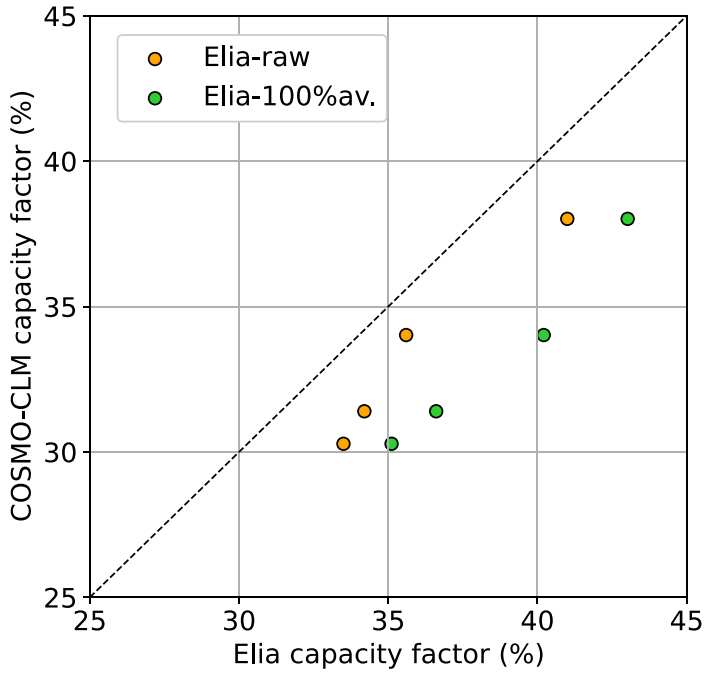

Figure A1. Comparison of the 4 annual capacity factors computed from Elia data and from the best-match of the annual subsets of the COSMO-CLM simulation, after correcting the latter for the mismatch in the annual wind speed distribution. Orange markers: raw Elia data uncorrected for downtime/curtailment. Green markers: Elia data corrected to 100% availability, as is assumed in the COSMO-CLM simulations.

Appendix B. Comparison with energy production data for the Belgian cluster

The Belgian transmission system operator Elia makes aggregated energy production data available for the operational Belgian wind farm cluster at 15 min intervals [62]. Here, we compare the annual energy output of the Belgian wind farms derived from the WF24 simulation with this data. We only consider the Elia data of 2021–2024, because our fixed WF24 wind farm distribution for this region is in agreement with the actual wind farm distribution over that period. As our simulations were conducted for the climate of 2000–2009, we selected a best match from the annual subsets of the COSMO-CLM simulation for each of the years of the 2021–2024 period based on the agreement between annual ERA5 wind roses (e.g. 2022 and 2006). As the match in the wind speed distribution was not perfect, the COSMO-CLM-derived capacity factor for the selected year was corrected with the capacity factor difference derived from ERA5 annual wind speed distributions for the two years after processing with the power curve of the NREL 5MW RWT.

For each year of the Elia data, an annual downtime-curtailment correction factor was determined based on a co-analysis of hourly wind speeds from ERA5 in the Belgian North Sea and the Elia production data: capacity factors were computed for all instances where the ERA5 wind speed was in the 18–20 ms^{-1} range. Rated production is normally attained in this wind speed range and wake losses are assumed to be negligible, so that any deviation from a capacity factor of 100% is expected to be due to downtime and/or curtailment of turbines. These correction factors were then applied to the measured annual capacity factors in agreement with the COSMO-CLM simulations which assume 100% availability and no curtailment.

Figure A1 shows the comparison in annual capacity factors with the raw Elia data and with Elia data corrected for downtime and curtailment. Capacity factors from COSMO-CLM are on average 2.6%pt too low compared to the raw Elia data, which translates to an average underestimation of the AEP of 7.3%. Corrected for downtime and curtailment, the capacity factor is underestimated by 5.3%pt by COSMO-CLM. However, this increased availability would lead to stronger intra-farm wakes which would in turn reduce the capacity factor by 1.1%pt, which we estimate based on table 2. For the remaining underestimation, we estimate that 1.5%pt results from the background wind bias described in Borgers *et al* [19]. Therefore, COSMO-CLM appears to overestimate intra-farm wake deficits, leading to a 2.7%pt underestimation of the capacity factor, or 8.1% of AEP.

ORCID iDs

R Borgers https://orcid.org/0000-0002-8696-1261
J Meyers https://orcid.org/0000-0002-2828-4397
N P M van Lipzig https://orcid.org/0000-0003-2899-4046

References

[1] IPCC 2022 *Climate Change 2022: Mitigation of Climate Change. Contribution of Working Group III to the Sixth Assessment Report of the Intergovernmental Panel on Climate Change* (Cambridge University Press)
[2] IRENA 2024 Renewable capacity statistics 2024, International Renewable Energy Agency, Abu Dhabi (available at: www.irena.org/Publications/2024/Mar/Renewable-capacity-statistics-2024) (Accessed 13 May 2024)
[3] European Commission 2020 Communication from the Commission to the European Parliament, the Council, the European Economic and Social Committee and the Committee of the regions (available at: https://eur-lex.europa.eu/legal-content/EN/TXT/?uri=COM:2020:741:FIN&qid=1605792629666) (Accessed 13 May 2024)
[4] Ostend Declaration 2023 Ostend Declaration on the North Sea as Europe's Green Power Plant (available at: www.government.nl/documents/diplomatic-statements/2023/04/24/ostend-declaration-on-the-north-sea-as-europes-green-power-plant) (Accessed 1 June 2023)
[5] Geyer B, Weisse R, Bisling P and Winterfeldt J 2015 Climatology of North Sea wind energy derived from a model hindcast for 1958–2012 *J. Wind Eng. Ind. Aerodyn.* **147** 18–29
[6] Giddings J, Bloomfield H, James R and Blair M 2024 The impact of future UK offshore wind farm distribution and climate change on generation performance and variability *Environ. Res. Lett.* **19** 064022
[7] Westerhellweg A, Cañadillas B, Kinder F and Neumann T 2014 Wake measurements at alpha ventus—dependency on stability and turbulence intensity *J. Phys.: Conf. Ser.* **555** 012106
[8] Foreman R J, Cañadillas B and Robinson N 2024 The atmospheric stability dependence of far wakes on the power output of downstream wind farms *Energies* **17** 488
[9] Christiansen M B and Hasager C B 2005 Wake effects of large offshore wind farms identified from satellite SAR *Remote Sens. Environ.* **98** 251–68
[10] Platis A *et al* 2018 First *in situ* evidence of wakes in the far field behind offshore wind farms *Sci. Rep.* **8** 2163
[11] Munters W, Adiloglu B, Buckingham S and van Beeck J 2022 Wake impact of constructing a new offshore wind farm zone on an existing downwind cluster: a case study of the Belgian Princess Elisabeth zone using FLORIS *J. Phys.: Conf. Ser.* **2265** 022049
[12] Lanzilao L and Meyers J 2024 Wind-farm wake recovery mechanisms in conventionally neutral boundary layers (arXiv:2407.17198 [physics.flu-dyn])
[13] Fischereit J, Brown R, Larsén X G, Badger J and Hawkes G 2022 Review of mesoscale wind-farm parametrizations and their applications *Bound.-Layer Meteorol.* **182** 175–224
[14] Fischereit J, Larsén X G and Hahmann A N 2022 Climatic impacts of wind-wave-wake interactions in offshore wind farms *Front. Energy Res.* **10** 881459
[15] Wang Q, Luo K, Wu C, Tan J, He R, Ye S and Fan J 2023 Inter-farm cluster interaction of the operational and planned offshore wind power base *J. Clean. Prod.* **396** 136529
[16] Larsén X *et al* 2019 Linking calculation of wakes from offshore wind farm cluster to the Danish power integration system *Technical Report* (Technical University of Denmark) (Accessed 25 October 2021)

[17] Syed A H, Javed A, Feroz R M A and Calhoun R 2020 Partial repowering analysis of a wind farm by turbine hub height variation to mitigate neighboring wind farm wake interference using mesoscale simulations *Appl. Energy* **268** 115050
[18] Akhtar N, Geyer B, Rockel B, Sommer P S and Schrum C 2021 Accelerating deployment of offshore wind energy alter wind climate and reduce future power generation potentials *Sci. Rep.* **11** 11826
[19] Borgers R, Dirksen M, Wijnant I L, Stepek A, Stoffelen A, Akhtar N, Neirynck J, Van de Walle J, Meyers J and van Lipzig N P M 2024 Mesoscale modelling of North Sea wind resources with COSMO-CLM: model evaluation and impact assessment of future wind farm characteristics on cluster-scale wake losses *Wind Energy Sci.* **9** 697–719
[20] Pryor S C and Barthelmie R J 2024 Power production, inter- and intra-array wake losses from the U.S. east coast offshore wind energy lease areas *Energies* **17** 1063
[21] van der Laan M P, García-Santiago O, Sørensen N N, Troldborg N, Risco J C and Badger J 2023 Simulating wake losses of the Danish Energy Island wind farm cluster *J. Phys.: Conf. Ser.* **2505** 012015
[22] Baas P 2024 Winds of the North Sea in 2050- public final report *Technical Report* (Whiffle) (Accessed 8 August 2024)
[23] Rosencrans D, Lundquist J K, Optis M, Rybchuk A, Bodini N and Rossol M 2024 Seasonal variability of wake impacts on US mid-Atlantic offshore wind plant power production *Wind Energy Sci.* **9** 555–83
[24] Porchetta S, Howland M F, Borgers R, Buckingham S and Munters W 2024 Annual wake impacts in and between wind farm clusters modelled by a mesoscale numerical weather prediction model and fast-running engineering models *Wind Energy Sci. Discuss.* **2024** 1–37
[25] Li D, Geyer B and Bisling P 2016 A model-based climatology analysis of wind power resources at 100-m height over the Bohai Sea and the Yellow Sea *Appl. Energy* **179** 575–89
[26] Nolan P, Lynch P and Sweeney C 2014 Simulating the future wind energy resource of Ireland using the COSMO-CLM model *Wind Energy* **17** 19–37
[27] Reyers M, Moemken J and Pinto J G 2016 Future changes of wind energy potentials over Europe in a large CMIP5 multi-model ensemble *Int. J. Climatol.* **36** 783–96
[28] Santos J A, Rochinha C, Liberato M L R, Reyers M and Pinto J G 2015 Projected changes in wind energy potentials over Iberia *Renew. Energy* **75** 68–80
[29] Neirynck J, Van de Walle J, Borgers R, Jamaer S, Meyers J, Stoffelen A and van Lipzig N P M 2024 Mesoscale weather systems and associated potential wind power variations in a midlatitude sea strait (Kattegat) *Wind Energy Sci.* **9** 1695–711
[30] Akhtar N, Geyer B and Schrum C 2022 Impacts of accelerating deployment of offshore windfarms on near-surface climate *Sci. Rep.* **12** 18307
[31] Chatterjee F, Allaerts D, Blahak U, Meyers J and van Lipzig N P M 2016 Evaluation of a wind-farm parametrization in a regional climate model using large eddy simulations *Q. J. R. Meteorol. Soc.* **142** 3152–61
[32] Fitch A C, Olson J B, Lundquist J K, Dudhia J, Gupta A K, Michalakes J and Barstad I 2012 Local and mesoscale impacts of wind farms as parameterized in a mesoscale NWP model *Mon. Weather Rev.* **140** 3017–38
[33] Ali K, Schultz D M, Revell A, Stallard T and Ouro P 2023 Assessment of five wind-farm parameterizations in the weather research and forecasting model: a case study of wind farms in the North Sea *Mon. Weather Rev.* **151** 2333–59
[34] Fischereit J, Vedel H, Larsén X G, Theeuwes N E, Giebel G and Kaas E 2024 Modelling wind farm effects in HARMONIE–AROME (cycle 43.2.2)—part 1: implementation and evaluation *Geosci. Model Dev.* **17** 2855–75
[35] Dirksen M, Wijnant I, Siebesma P, Baas P and Natalie T 2022 Validation of wind farm parameterisation in weather forecast model HARMONIE-AROME—analysis of 2019 *Technical Report* (Delft University of Technology) (Accessed 1 September 2022)
[36] Garcia-Santiago O M, Badger J, Hahmann A N and da Costa G L 2022 Evaluation of two mesoscale wind farm parametrisations with offshore tall masts *J. Phys.: Conf. Ser.* **2265** 022038
[37] Fischereit J, Hansen K S, Larsén X G, van der Laan M P, Réthoré P-E and Leon J P M 2021 Comparing and validating intra-farm and farm-to-farm wakes across different mesoscale and high-resolution wake models *Wind Energy Sci. Discuss.* **7** 1–31
[38] EMODnet 2023 Wind farms (polygons) (EMODnet Human Activities) (available at: https://emodnet.ec.europa.eu/en/human-activities#humanactivities-data-products) (Accessed 30 January 2023)
[39] Vigin L 2022 Shapefiles of the Belgian and Dunkirk offshore zones (available at: www.bmdc.be/NODC/index.xhtml) (Accessed 19 January 2022)
[40] Hahmann A N, García-Santiago O and Peña A 2022 Current and future wind energy resources in the North Sea according to CMIP6 *Wind Energy Sci.* **7** 2373–91
[41] Slavik K, Lemmen C, Zhang W, Kerimoglu O, Klingbeil K and Wirtz K W 2019 The large-scale impact of offshore wind farm structures on pelagic primary productivity in the southern North Sea *Hydrobiologia* **845** 35–53
[42] Li C, Mogollón J M, Tukker A, Dong J, von Terzi D, Zhang C and Steubing B 2022 Future material requirements for global sustainable offshore wind energy development *Renew. Sustain. Energy Rev.* **164** 112603
[43] Jadali A M, Ioannou A, Salonitis K and Kolios A 2021 Decommissioning vs. repowering of offshore wind farms—a techno-economic assessment *Int. J. Adv. Manuf. Technol.* **112** 2519–32
[44] van Stratum B, Theeuwes N, Barkmeijer J, van Ulft B and Wijnant I 2022 A one-year-long evaluation of a wind-farm parameterization in HARMONIE-AROME *J. Adv. Model. Earth Syst.* **14** e2021MS002947
[45] Jonkman J, Butterfield S, Musial W and Scott G 2009 Definition of a 5-MW reference wind turbine for offshore system development *Technical Report* No. NREL/TP-500-38060 (National Renewable Energy Lab. (NREL))
[46] Bak C, Zahle F, Bitsche R, Kim T, Yde A, Henriksen L C, Hansen M H, Blasques J P A A, Gaunaa M and Natarajan A 2013 The DTU 10-MW reference wind turbine (available at: https://orbit.dtu.dk/en/publications/the-dtu-10-mw-reference-wind-turbine) (Accessed 6 May 2022)
[47] Gaertner E *et al* 2020 IEA wind TCP task 37: definition of the IEA 15-megawatt offshore reference wind turbine *Technical Report* No. NREL/TP-5000-75698 (National Renewable Energy Lab. (NREL))
[48] Bento N and Fontes M 2019 Emergence of floating offshore wind energy: technology and industry *Renew. Sustain. Energy Rev.* **99** 66–82
[49] Shields M, Beiter P, Nunemaker J, Cooperman A and Duffy P 2021 Impacts of turbine and plant upsizing on the levelized cost of energy for offshore wind *Appl. Energy* **298** 117189
[50] Borrmann R, Knud R, Wallasch A-K and Lüers S 2018 Capacity densities of European offshore wind farms *Technical Report* (Deutsche WindGuard GmbH) (Accessed 2 February 2022)
[51] Badger J, Imberger M, Volker P, Kleidon A, Germer S and Minz J 2020 Making the most of offshore wind: re-evaluating the potential of offshore wind in the German North Sea *Technical Report* (Technical University of Denmark and Max-Planck-Institute of Biogeochemistry) (Accessed 2 February 2022)
[52] Borgers R 2024 Wind farm scenarios for the North Sea for 2024 and 2030 (KU Leuven Research Data Repository) (https://doi.org/10.48804/HHD0WL) (Accessed 29 October 2024)

[53] García-Santiago O, Hahmann A N, Badger J and Peña A 2024 Evaluation of wind farm parameterizations in the WRF model under different atmospheric stability conditions with high-resolution wake simulations *Wind Energy Sci.* **9** 963–79
[54] Stieren A and Stevens R J A M 2021 Evaluating wind farm wakes in large eddy simulations and engineering models *J. Phys.: Conf. Ser.* **1934** 012018
[55] Pryor S C, Shepherd T J, Volker P J H, Hahmann A N and Barthelmie R J 2020 'Wind theft' from onshore wind turbine arrays: sensitivity to wind farm parameterization and resolution *J. Appl. Meteorol. Climatol.* **59** 153–74
[56] BBC 2023 Norfolk Boreas: work on offshore wind farm stops over soaring costs (available at: www.bbc.com/news/uk-england-norfolk-66263340) (Accessed on 23 October 2023)
[57] Dogger Bank Wind Farm 2025 Building the world's largest offshore wind farm (available at: https://doggerbank.com/) (Accessed 22 March 2025)
[58] Foloppe B, Dewitte L and Munters W 2023 Exploring cooperation between wind farms: a wake steering optimization study of the Belgian offshore wind farm cluster *J. Phys.: Conf. Ser.* **2505** 012055
[59] Finserås E, Anchustegui I H, Cheynet E, Gebhardt C G and Reuder J 2024 Gone with the wind? Wind farm-induced wakes and regulatory gaps *Mar. Policy* **159** 105897
[60] FREEWIND 2024 Website of the FREEWIND project (available at: https://freewind-project.eu/)
[61] Borgers R 2024 Fitch wind farm parametrization in COSMO5-CLM15—V3 *Zenodo* https://doi.org/10.5281/zenodo.12547570 (Accessed 26 June 2024)
[62] Elia Transmission Belgium SA 2025 Wind power production estimation and forecast on Belgian grid (Historical) (available at: https://opendata.elia.be/explore/dataset/ods031/information/) (Accessed 12 January 2025)